Serial Robotic Arm Joint Characterization Measurements for Antenna Metrology

Michael S. Allman, David Novotony,
Joshua Gordon, Alex Curtin
Communications Technology Laboratory
National Institute of Standards and Technology
Boulder, CO, USA
mallman@nist.gov

Scott Sandwith
New River Kinematics
Williamsburg, VA, USA
scott@kinematics.com

***Abstract*— We improved the accuracy of our six-axis serial robotic arm used for antenna characterization measurements by calibrating a kinematic robot model based on our robot's physical dimensions. The model was calibrated over a 0.4 m^3 working cell. We validated the calibration using a 1 m^2 plane embedded within the calibration cell. The positioning errors for the calibrated case showed a fourfold improvement in accuracy as compared to the uncalibrated case. For a maximum positioning error tolerance of $\lambda/50$, the calibrated model should allow for open-loop antenna characterization measurements up to 35 GHz.**

***Keywords*— Antennas, near-field measurements, positioning, gain, pattern.**

I. Introduction

The accurate alignment of antennas and field probes is a critical aspect of modern antenna metrology systems, particularly in the millimeter-wave region of the spectrum, [1,2,3]. Commercial off-the-shelf robotic arms provide a sufficient level of positional accuracy for many industrial applications [4]. However, to be useful for millimeter-wave antenna metrology, robotic arms need to be operated in conjunction with spatial metrology equipment. The Antenna Metrology Project in the Communications Technology Laboratory at the National Institute of Standards and Technology has shown that path-corrected commercial robotic arms, both in hardware and software analysis, can be used to achieve sufficient positioning and alignment accuracies (positioning error ~ $\lambda/50$) for antenna characterization measurements such as gain extrapolation and near-field pattern up to 183 GHz [3].

The robot used in this work is a six-axis serial robotic arm. Each link is manipulated by a revolute joint. Starting at the base of the robot and working toward the end link, the joints are labeled (Fig 2.) J0: Base, J1: Sweep (S), J2: Lower (L), J3: Upper (U), J4: Roll (R), J5: Bend (B), J6: Twist (T). The orientation of each link is described by a conceptual coordinate system, called a "link frame", firmly affixed to each link [5]. Attached to the T joint is a flange that allows the attachment of the robot "end effector." The end effector can be any object that performs some function (e.g. drill, welder, mechanical gripper, laser, probe antenna etc.). At some location on the end effector, exists the tool control point (TCP) frame. This frame defines the robot's position and orientation. The robot controller uses a kinematic model to calculate the joint angles required to move the TCP to a commanded position and orientation in space. In this work, the accuracy of the robot refers to the relative error (both offset and orientation) between the robot's commanded TCP position and the actual TCP position. This error is directly related to the accuracy of the parameters that comprise the kinematic model used by the controller.

There are two methods to compensate the robot position accuracy performance. First, a spatial metrology system, in this case a laser tracker with a 6-degree-of-freedom (6DOF)

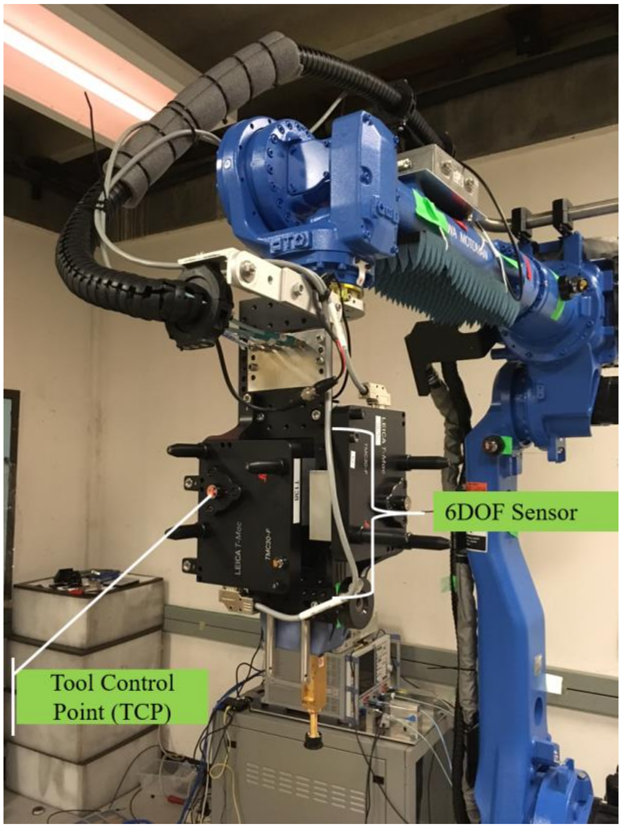

Figure 1. Robot showing end effector and TCP location.

sensor acting as the robot's TCP (Fig. 1), can be used to iteratively correct the robot's TCP position until it is within tolerance of its goal position and orientation [3,6]. This technique is called Move-Measure-Correct (MMC). When using the MMC technique, the TCP's actual position is measured using the laser tracker and compared to its commanded goal position as the TCP moves through its intended path. A real-time path correction based on these comparisons is iteratively applied to the robot until the desired level of accuracy is achieved in the frequency range of interest. This "closed loop" method of robot motion control results in the most accurate TCP positioning and requires minimal a priori knowledge of the robot link frames, but requires that the positioning metrology system constantly monitor the TCP position during the measurement. In an actual antenna measurement, the TCP would reside centered on the aperture of a probe antenna, requiring knowledge of an additional frame transformation between the 6DOF sensor and the TCP. We already have an accurate means for measuring that transformation [7].

At lower frequency ranges (< 40 GHz), a second method to improve positioning accuracy can be employed where the metrology system is used to acquire a calibrated model of the robot [6, 8]. This technique has the advantage that after the calibration is performed and used to compute accurate robot poses, the metrology system is not needed in the cell to provide real-time path corrections while the robot is in motion. However, the success of this approach hinges on improved knowledge of the robot link frame transforms. This paper will focus on the calibration process and results using this second "open loop" technique to improve robot accuracy.

The complete calibrated robot model can be divided into two sets of parameters. The first set, referred to here as an extrinsic calibration, establishes the robot base frame and TCP transforms (Fig 2). The second, intrinsic, set of parameters establishes an improved kinematic model of the robot. In other words, the extrinsic calibration solves for where the robot is relative to the world frame and the intrinsic calibration optimizes the robot's kinematic model. The kinematic model is based on knowledge of the link frame transformations between adjacent links and can also model deviations due to gravitational loading on the joints and small mechanical offsets between the joints. Each link frame, *i*, is described by four physical quantities, known as Denavit-Hartenberg (DH) parameters [5]:

- a_i is the length of the common normal line between the ith and (i+1)th joint rotation axes. These axes also define Z_i and Z_{i+1} respectively.
- α_i is the angle between Z_i and Z_{i+1} as a rotation about X_i.
- d_i is the distance between X_{i-1} and X_i as measured along Z_i.
- θ_i is the angle from X_{i-1} to X_i as a rotation about Z_i.

The parameter, a_i, is commonly referred to as the "link length", parameter, α_i, the "twist angle", parameter d_i, the "length offset", and parameter θ_i, the "joint angle." The

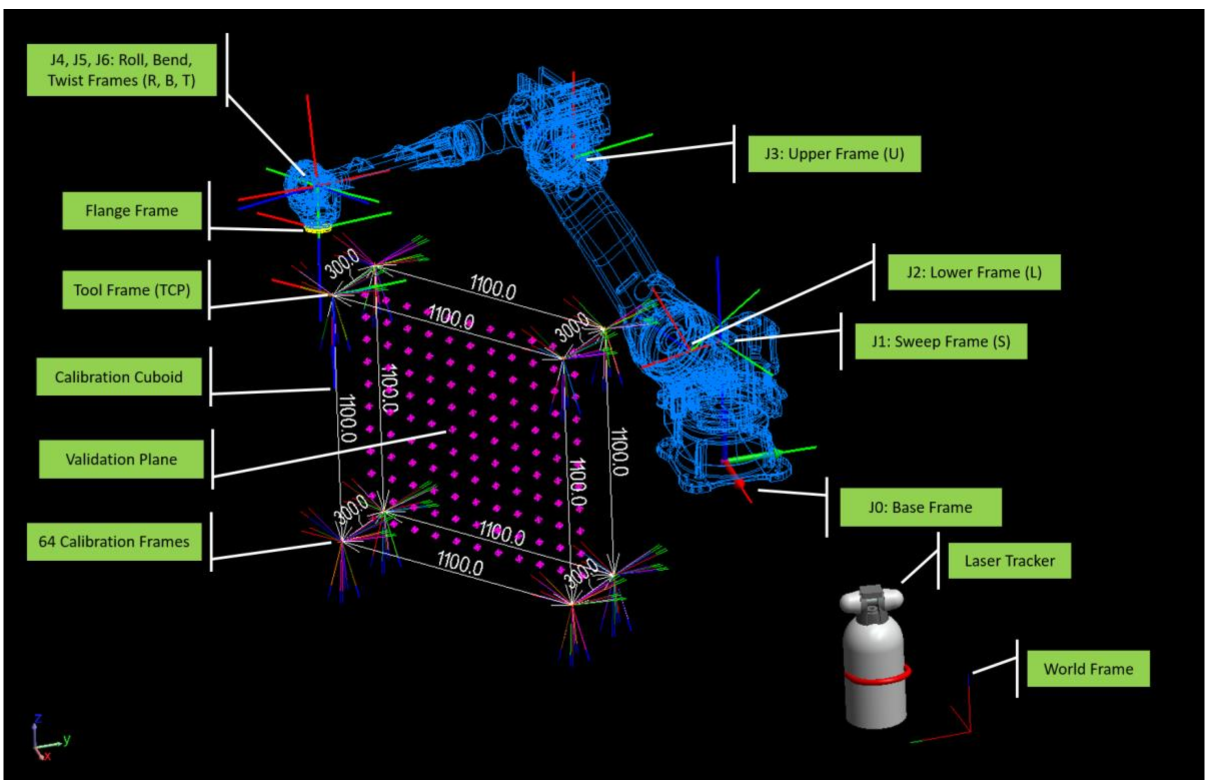

Figure 2: Screen capture of robot CAD model and calibration cell. The laser tracker and relevant frames are labeled. The units are millimeters.

transform between the (i-1)th and ith link frame in terms of the DH parameters is:

$$
{}^{i-1}_{i}T = \begin{bmatrix} \cos(\theta_i) & -\sin(\theta_i) & 0 & a_{i-1} \\ \sin(\theta_i)\cos(\alpha_{i-1}) & \cos(\theta_i)\cos(\alpha_{i-1}) & -\sin(\alpha_{i-1}) & -d_i\sin(\alpha_{i-1}) \\ \sin(\theta_i)\sin(\alpha_{i-1}) & \cos(\theta_i)\sin(\alpha_{i-1}) & \cos(\alpha_{i-1}) & d_i\cos(\alpha_{i-1}) \\ 0 & 0 & 0 & 1 \end{bmatrix} \quad (1)
$$

Robot joint-link deflection is modeled as rotation about the link XYZ axes respectively as a linear torsional spring constant. The deflection is compensated by computing a joint angle to counter the deflection based on load and robot pose. Although our calibration software can model deflection, the focus of the work presented here was to investigate the accuracy limits of our robot with a simpler kinematic model that does not account for gravity.

II. Calibration Procedure

A. *Software*

For the calibration procedure, we wrote a custom software application called "NIST Robot Calibrator (NRC)" to interface with the robot controller and New River Kinematics Spatial Analyzer (SA) Machine Software†. NRC provides an easy-to-use automated software development kit (SDK) interfaced into SA's robot calibration functionality to configure and solve for the robot calibration in our test range. Additionally, the NRC application automates measurement configuration and acquisition for the laser tracker and interfaces to the robot controller to automate manipulating the physical robot.

A complete, nominal kinematic SA model of the robot was developed based on CAD models from the robot manufacturer. This robot model provided nominal joint-link frame parameters (DH parameters) as well as a method to visualize robot motion in SA. Fig. 2 shows the robot model and the link frames laid over the CAD model from the robot manufacturer.

B. *Calibration Cell*

Using the NRC software, we defined the corners of a cuboid in SA. Centered on each of these 8 corners, 8 virtual frames were created at orientations of +/- 20 degrees about each axis of rotation. The orientations of the corner frames had to be chosen carefully so that the 6DOF sensor remained in view of the laser tracker for all the calibration poses. We then commanded the robot model to align its TCP frame with each of the 64 frames. Sets of robot joint angles for each frame where then computed using inverse kinematics based on the relative position of the robot base and the SA model of the robot. The physical robot was moved to each joint set where the actual position of the TCP was measured by the spatial metrology system and the actual joint encoder count was read from the robot controller. Encoder counts were converted to joint degrees. The resulting measured TCP frames and the achieved joint angles for each pose were fed into SA's kinematic optimization routine that outputs offsets to correct the intrinsic and extrinsic robot parameters such that the errors between the TCP's target poses and achieved poses were minimized.

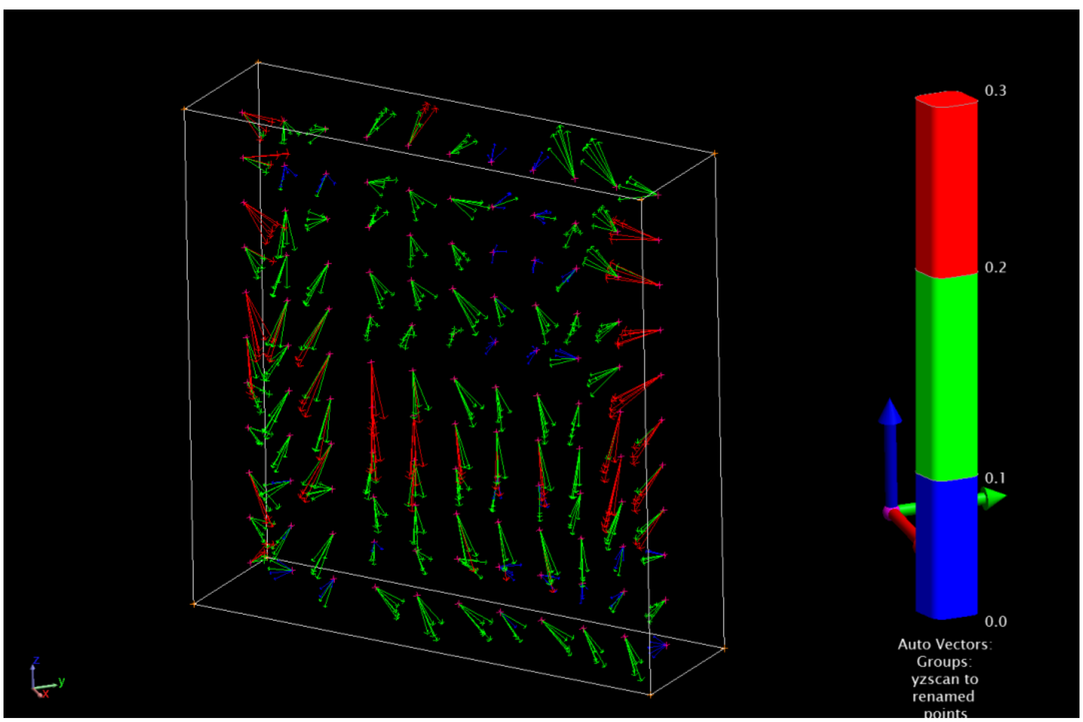

Figure 3. Calibration validation over 1 m^2 planar surface. Five separate validation results are shown. The error vectors are magnified 500 X. The green vectors are within 1 std of the mean. The red vectors are above the mean. The blue vectors are below the mean. The units are millimeters.

† Mention of this product is not an endorsement but only serves to clarify what was done in this work.

C. Two-Step Calibration

The calibration was performed in two steps. The first step was an extrinsic calibration to position the robot model's base frame to within a few millimeters of its physical lab location with respect to the laser tracker. Initially, the robot model was aligned to the default world frame whose orientation with respect to the laser tracker is arbitrary. Additionally, the robot model's initial TCP frame transform with respect to the end link was set to zero. The initial calibration was performed using a cubic calibration cell of volume ~1/8 m^3; centered in front of the robot. Once the robot model's base and TCP transforms were roughly aligned to the laser tracker, we adjusted the calibration cell so that we could validate the calibration using a planar surface, nominally $1m^2$ in area embedded inside the cuboid. We biased the cuboid to the (+X,-Y,+Z) quadrant of the robot's base frame (shown in Fig. 2) to keep the robot's center of gravity forward of the robot base while keeping the 6DOF target beyond the laser tracker's 1.5 m minimum range limit. Figure 2 shows the calibration cuboid with virtual pose frames at each corner.

D. Choosing Fit Parameters

Depending on the range of motion of each robot joint pose used in the calibration, some fit parameters may be dependent on each other. In fact, some parameters will always be dependent. For example, an offset in the θ DH parameter for the S link frame (S(θ), Fig. 2) can always be perfectly negated by an offset Z-rotation of the robot base frame ($Base(R_z)$). Thus S(θ) and $Base(R_z)$ should never be included together in the optimization. Additionally, any link frame whose Z rotation axis is nominally parallel to the previous link's Z rotation axis should not include the link offset parameter (d) in the fit, since there exists an infinite number of possible link offsets that can be chosen for that link configuration. Determining the best subset of DH parameters to optimize over in a given calibration cell is part of the "art" of acquiring a good kinematic model of the robot. The correlation matrix between the fit parameters (automatically generating by SA) provides good insight into which parameters are too strongly correlated to be fit simultaneously. Table 1 lists the link parameters that were fit.

TABLE 1. DH Parameters optimized in calibration.

Joint	**DH Parameter**			
	α	***A***	***d***	***θ***
S				
L	✓	✓	✓	✓
U	✓	✓		✓
R	✓	✓	✓	✓
B		✓	✓	✓
T	✓	✓		

E. Optimization Results

The initial DH values used in the kinematic solver were a combination of nominal values reported by the robot manufacturer and values that we could directly measure in the lab. By moving the joints S, L, U, and R independently while tracking their positions with the spatial metrology system, we could directly measure their link lengths or link offset (depending on the axis). The link lengths/link offsets for B and T could not be measured because their link frames nominally coincide. Table 2 lists the DH parameter starting values and the corrections output by the optimization routine for this calibration.

Table 2. DH parameter initial values and corrections

Joint	**DH Parameter**			
	α (deg)	a (mm)	d (mm)	θ (deg)
S (initial value)	0	0	540	0
S (correction)	n/a	n/a	n/a	n/a
L (initial value)	90.0000	144.967[a]	0	0
L (correction)	-0.0064	-2.4375	0.27615	0.11663
U (initial value)	0	1151.3155[a]	0	0
U (correction)	0.0218	0.4283	n/a	-0.0265
R (initial value)	90	210.5065[a]	1224.7863[a]	0
R (correction)	0.00133	-0.8884	0.2665	-0.0119
B (initial value)	90	0	0	0
B (correction)	n/a	-0.1858	-0.1618	-0.0317
T (initial value)	-90	0	0	90
T (correction)	0.0153	-0.0903	n/a	n/a

[a] Directly measured

The correction offset for DH parameter, a, for joint L seems excessive. Physically, this parameter describes the normal distance between the S and L rotation axes. We do not believe this distance to deviate from the nominal value by such a large degree. We suspect this offset is an indication that the robot kinematics could be improved by adding deflection to the model. Future work will attempt to verify if our suspicions are correct.

III. CALIBRATION VALIDATION

A. Validation Using Calibrated Model

We validated this calibration using a 1 m^2 planar grid of points embedded in the cuboid. The spacing between points was 100 mm. A grid of this type represents a typical near-field planar scan geometry. Fig. 2 shows the validation plane inside the cuboid. The TCP offset error vectors (magnified 500×) for five separate validation scans, taken on different days, are shown. The mean offset error magnitude of all five scans was 170 µm. The maximum offset error was 339 µm. The minimum offset error was 20 µm. The overall standard deviation was 64 µm. Table 3 lists the results for the individual scans.

TABLE 3. Calibrated model validation scan results

Scan	**Offset Error Magnitude (µm)**			
	Mean	**Std**	**Max**	**Min**
1	189	68	339	26
2	169	61	294	22
3	175	65	316	20
4	155	58	280	34
5	160	59	291	30

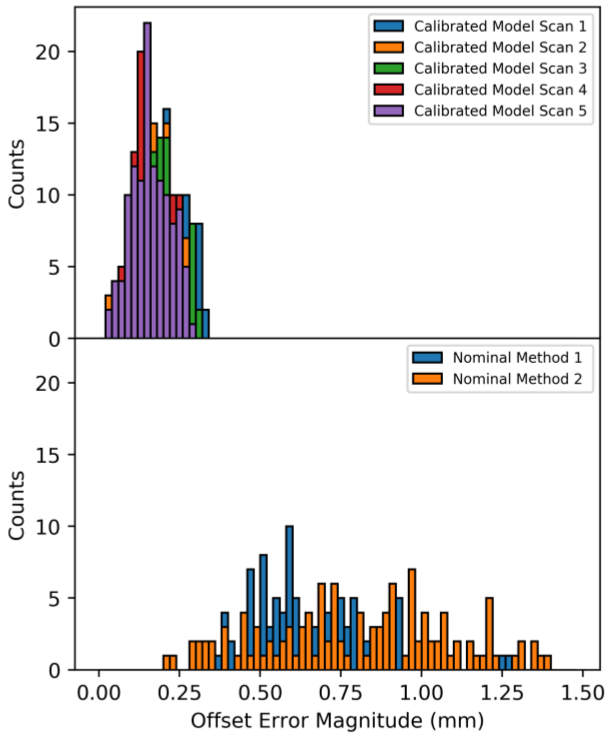

Figure 4. Offset error magnitudes of the validation scans for the calibrated model and the nominal robot model. The overall mean offset error magnitude was 170 µm with 64 µm standard deviation. The uncalibrated model mean offset error magnitude was 696 µm with a 225 µm standard deviation.

B. *Validation Using Nominal Model (For Comparison)*

1) Method 1 (Extrinsic Calibration)

We also performed the same validation scan using the nominal kinematic model of the robot using two different methods. For the first method, we performed only an extrinsic calibration of the robot model, fitting only the robot model's base and tool transform offsets and orientations. The DH parameters used in the kinematic model we held fixed at their nominal or lab-measured values. The scan poses were calculated using this partially calibrated model. These poses were applied to the physical robot and measured using the same validation plane for the fully-calibrated case.

2) Method 2 (Robot Controller Base Frame)

For the second method, we used the physical robot's internal base frame as the reference frame. To do this, we had to locate the physical robot's internal base frame in SA. This procedure involved two primary steps. We first input the tool offset into the robot controller using a tool alignment calibration procedure programmed into the robot controller. Once the tool parameters were set, we then drove the robot to a set of (X,Y,Z) positions with respect to the physical robot's internal base frame and measured these positions with the laser tracker. In SA, the measured frames were back-transformed using the coordinate values reported by the robot controller. The resulting cluster of frames centered on the physical robot's base frame location in SA was then averaged. Once this frame was set in SA, the validation coordinates with respect to the physical robot's base frame were programmed into the robot controller and measured. The purpose of this lengthy second method of uncalibrated validation was to simulate how a user would typically perform a planar scan without the benefit of robot calibration software

3) Results

Table 4 lists the results of the method 1 and method 2 uncalibrated scans. Fig. 4 shows histograms of the validation scan plane offset error magnitudes for the calibrated and uncalibrated validation scans. In Fig. 5 histograms of the (X,Y,Z) projections of the offset errors in the robot base frame coordinate system are shown for calibrated model scan 1 and nominal model method 1. The X and Y components showed the largest improvement with the calibration. The Z components showed essentially no difference between the calibrated and nominal model. Fig.6 shows the orientation errors for the same scans shown in Fig. 5. These orientations are with respect to the target frame at each validation plane point. For each validation point, only a single frame was used. To calculate the orientation of the measured frame with respect to the nominal target frame, first an X rotation (R_x) is performed, then a Y rotation (R_y), then a Z rotation (R_z) about the nominal frame X,Y, and Z axes. Table 5 lists the mean orientation errors. The uncertainties are 1 std values.

TABLE 4. Uncalibrated validation scan results.

Scan	Offset Error Magnitude (µm)			
	Mean	Std	Max	Min
Method 1	694	228	1311	320
Method 2	803	288	1397	203

TABLE 5. Orientation errors.

Rotation Axis	Orientation Error (degrees)	
	Calibrated	Uncalibrated
R_x	$(5.3 \pm 9.8) \times 10^{-3}$	$(10.0 \pm 15.4) \times 10^{-3}$
R_y	$(4.0 \pm 6.1) \times 10^{-3}$	$(-0.7 \pm 17.0) \times 10^{-3}$
R_z	$(-2.7 \pm 13.8) \times 10^{-3}$	$(0.0 \pm 14.1) \times 10^{-3}$

C. Mechanical Hysteresis

Some level of mechanical hysteresis is always present when dealing with positional manipulators and our robot is no different. Intuitively, we expect the degree of hysteresis to be a limiting factor in achievable positioning accuracy. We measured the hysteresis for each joint by performing repeated movements of each link to a nominal position from opposing directions. The measured points from each direction were averaged and the distance between the averaged points was divided by the radial distance of the averaged point to the axis of rotation. Table 6 lists our backlash measurements. The combined cluster of measured points was averaged resulting in an RMS deviation of 91 μm. Thus, we expect this value to be close to the ultimate accuracy limit achievable with our robot for bi-directional joint movement.

Table 6. Joint mechanical hysteresis measurements.

Joint	Hysteresis (deg)
S	$(8.6 \pm 0.4) \times 10^{-3}$
L	$(1.4 \pm 0.4) \times 10^{-3}$
U	$(1.6 \pm 0.2) \times 10^{-3}$
R	$(8.0 \pm 0.6) \times 10^{-3}$
B	$(14.8 \pm 1.0) \times 10^{-3}$
T	$(46.4 \pm 2.2) \times 10^{-3}$

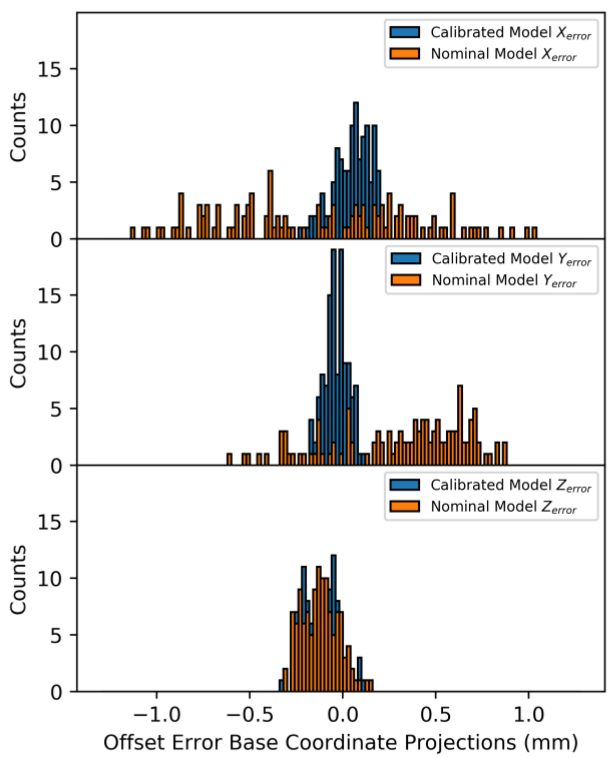

Figure 5: XYZ projections of the offset error in the robot base coordinate system. The X and Y components showed the largest improvement using the calibrated model. The Z component showed essentially no improvement.

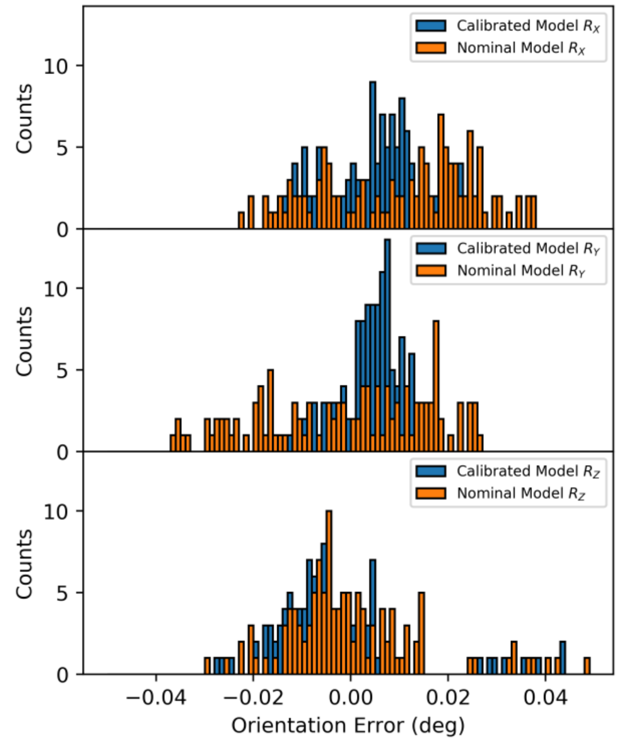

Figure 6. Orientation errors with respect to the nominal target frame for calibrated and uncalibrated validation scans.

IV. Conclusion

In summary, we have developed a calibrated kinematic model of our six-axis robot using an optimization routine provided by SA. We developed custom software to interface with SA and the robot controller, that provides a simple user interface to create a custom calibration cell, automate robot motion, calculate robot pose joint angles and configure the spatial metrology system. Using our custom software interface, we performed an intrinsic and extrinsic calibration of our robot over a 0.4 m^3 cell. We validated the calibration using a 1 m^2 planar grid embedded within the calibration cell and compared the TCP offset and orientation errors with the same measurements using an uncalibrated model. We also measured the mechanical hysteresis of each joint to get an estimate of the ultimate achievable accuracy of the calibrated robot. Our calibrated model showed a fourfold improvement in accuracy compared to the uncalibrated model. Using a maximum positioning tolerance error of λ/50, the calibrated robot model should allow for open loop antenna characterization measurements up to approximately 35 GHz. Future work will investigate accuracy improvements by adding gravitational deflection to the kinematic model. Additionally, we will test the dynamic accuracy of the calibrated robot model.

References

[1] J. Hatzis, P. Pelland, G. Hindman, "Implementation of a Combination Planar and Spherical Near-Field Antenna Measurement System using an

Industrial 6-Axis Robot" Proceedings of the Antenna Measurements Techniques Association, pp 416-422, 2016

[2] F. Ferrero, Y. Benoit, L. Brochier, J. Lanteri, J-Y Dauvignac, C. Migliaccio, S. F. Gregson, "Spherical Scanning Measurement Challenge for Future Millimeter Wave Applications" Proceedings of the Antenna Measurements Techniques Association, 2015

[3] D. R. Novotny, J.A. Gordon, J.R. Guerrieri, "Antenna Alignment and Positional Validation of a mm Wave Antenna System Using 6D Coordinate Metrology, " Proceedings of the Antenna Measurements Techniques Association, pp 247-252, 2014

[4] J. Sulzer, I. Kovac, "Enhancement of Positioning Accuracy of Industrial Robots with a Reconfigurable Fine-Positioning Module," Precision Engineering, vol. 34, pp 201-217, 2010

[5]. J.J. Craig, "Introduction to Robotics: Mechanics and Control, 3rd ed.," New Jersey, Prentice Hall, 2004, pp. 62-69

[6] R. Swanson, G. Balandran, S. Sandwith, "50-micron Hole Position Drilling Using Laser Tracker Controlled Robots, " Journal of the CMSC, Vol 9, No 1, Spring 2014

[7] J.A. Gordon, D.R. Novotny, M.H. Francis, R.C. Wittman, M.R. Butler, A.E. Curtin, J.R. Guerrieri, "Millimeter-Wave Near-Field Measurements Using Coordinated Robotics," IEEE Transactions on Antennas and Propagation, vol. 63, no. 12, pp 5351-5362, 2015

[8] A. Nubiola, I.A. Bonev, "Absolute calibration of an ABB IRB 1600 robot using a laser tracker," Robotics and Computer-Integrated Manufacturing, vol. 29, issue 1, pp 236-245, 201